GEOPHYSICS, VOL. 72, NO. 5 (SEPTEMBER-OCTOBER 2007); P. SM251–SM259, 19 FIGS.
10.1190/1.2749570

Seismic modeling of gas chimneys

Børge Arntsen[1], Lars Wensaas[1], Helge Løseth[1], and Christian Hermanrud[1]

ABSTRACT

We propose a simple acoustic model explaining the main features of gas chimneys. The main elements of the model consist of gas diffusing from a connected fracture network and into the surrounding shale creating an inhomogeneous gas saturation. The gas saturation results in an inhomogeneous fluctuating compressional velocity field that distorts seismic waves. We model the fracture network by a random-walk process constrained by maximum fracture length and angle of the fracture with respect to the vertical. The gas saturation is computed from a simple analytical solution of the diffusion equation, and pressure-wave velocities are locally obtained assuming that mixing of shale and gas occurs on a scale much smaller than seismic wavelengths. Synthetic seismic sections are then computed using the resulting inhomogeneous velocity model and shown to give rise to similar deterioration in data quality as that found in data from real gas chimneys. Also, synthetic common-midpoint (CMP) gathers show the same distorted and attenuated traveltime curves as those obtained from a real data set. The model shows clearly that the features of gas chimneys change with geological time (a model parameter in our approach), the deterioration of seismic waves being smallest just after the creation of the gas chimney. It seems likely that at least some of the features of gas chimneys can be explained by a simple elastic model in combination with gas diffusion from a fracture network.

INTRODUCTION

Vertical zones of deteriorated seismic data quality are found on data from several chalk fields of the Central North Sea, such as Albuskjell (D'Heur, 1987), Ekofisk (Pekot and Gregory, 1987), Eldfisk (Michaud, 1987), Hod (Norbury, 1987), Tommeliten (D'Heur and Pekot, 1987; see also Figure 1) and Valhall (Muns, 1985). These zones of deteriorated seismic data quality are often referred to as gas chimneys. The presence of gas chimneys have been interpreted as hydrocarbon leakage pathways, and mapping of such chimneys by neural network techniques has been established as an exploration tool (Meldahl et al., 2002; Ligtenberg, 2003; Heggland, 2004).

The disturbed seismic data quality is associated with reduced acoustic velocities (Dangerfield, 1992) and gas presence in overburden rocks (Muns, 1985). The influence of gas on the seismic image was further confirmed by Granli et al. (1999), who described imaging through the gas chimney above the Tommeliten Alpha field using marine shear wave data.

Shear waves show little interaction with fluids and were expected to penetrate gas-filled sediments without being significantly disturbed. The imaging of the overburden rocks improved significantly along the edges of the chimney (where the raypaths of the downward moving compressional waves did not pass through the chimney, but the raypaths of the upward-moving shear waves did).

Gas presence in sediments alone does not lead to deteriorated seismic signals, and the seismic imaging within and below gas-filled reservoirs are not in general poorer than outside gas-filled reservoirs. Deterioration of seismic signals because of gas presence is thus dependent on a specific distribution of gas within the sediments.

A theoretical model for acoustic wave propagation through partially gas-saturated sediments was proposed by White (1975). This model predicts strong attenuation of seismic waves caused by interaction of fluid flow with the elastic waves, and requires inhomogeneous gas saturation on a scale of a few centimeters to yield significant attenuation.

An alternative model by Lerche (1986) uses an acoustic medium with randomly fluctuating gas saturation on a scale of the seismic wavelength to predict properties of seismic waves propagating through gas chimneys. He relates the fluctuating gas saturation to fluctuations in the seismic velocity and derives analytical solutions of the resulting wave equation. The key observation here is that increasing gas saturation reduces compressional wave velocity, and even small amounts of gas imply a significant reduction in compressional-wave velocity.

O'Brien et al. (1999) uses a detailed velocity model to simulate the seismic effect of the gas chimney at the Valhall field. This model is based on the perceived existence of layers with low and laterally variant velocity. Synthetic seismic data reproducing the observed

Manuscript received by the Editor November 29, 2006; revised manuscript received March 8, 2007; published online August 23, 2007.
[1]Statoil, Trondheim, Norway. E-mail: barn@statoil.no; lawe@statoil.no; heloe@statoil.no; che@statoil.no

disturbed seismic imaging are obtained using a purely elastic model without introducing intrinsic attenuation.

While the conditions for deterioration of seismic signals caused by gas presence in the sediments thus seem to be well established, descriptions of geologic processes that can produce the required gas distribution, and modeling of the velocity variations that result from such processes, appear to be lacking. The purpose of this paper is to investigate the impact of gas leakage through caprock fracture networks on seismic velocities, and to evaluate to what extent such leakage can explain the seismic images that characterize the seismic chimneys above a large number of chalk fields in the Central Graben of the North Sea. Data from the Tommeliten Alpha field will provide a basis for comparing observations with modeling results.

GEOLOGIC DESCRIPTION

The Central Graben area is located in the intracratonic North Sea sedimentary basin. The main geologic features of this area have been known for some time and were summarized in *The Millennium Atlas* (Fraser et al., 2002). The most important geologic events of the area were the following: Caledonian basement rocks were overlain by clastic rocks of the Devonian and Permian periods. These rocks were superseded by the Late Permian Zechstein group, consisting of several cycles of evaporitic deposits, with massive salt deposits toward the top of each cycle. Clastic sediments of the Mesozoic era and Early Cretaceous age overlay these deposits, including Upper Jurassic shales of the Tau formation that serve as source rocks for the chalk fields.

The chalk deposits of late Cretaceous and Early Tertiary age are prolific reservoir rocks, and Tertiary and Quaternary shales and mudstones form efficient seals for these deposits. Salt diapirism created structural closures for the chalk fields, and resulted in fractures and nonzero permeability of these otherwise tight rocks. The timing of the latest salt movement varies among the individual diapirs, and some diapirs have been active as late as in Pleistocene times. The diaper movement below the Tommeliten Alpha structure was apparently active until the early Miocene.

The Tommeliten Alpha field was discovered in 1977. It has been penetrated by four wells, and is thought to contain 8.0×10^3 m^3 of oil and 13.0×10^9 m^3 of gas. The field is currently in the planning phase. The seismic chimney above the Tommeliten Alpha field extends from the Middle Miocene to well below the Cretaceous reservoir rocks (Figure 1). CMP gathers within the seismic chimney, shown in Figure 2, display no coherent signals, whereas gathers from just outside the chimney show well-behaved amplitudes with offset.

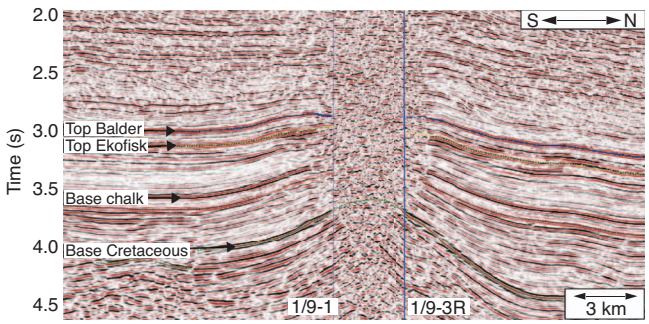

Figure 1. The Tommeliten Alpha gas chimney (from Granli et al., 1999).

A comparison between a well drilled just outside the chimney (Well 1/9-1) and a well drilled within the chimney (Well 1/9-3R) (Figure 3) shows that (1) the bulk density of the overburden rocks is the same, (2) the sonic velocity of the well within the chimney is significantly less that in the sediments outside the chimney, and (3) the mud gas readings in the sediments within the chimney testify to several intervals with high gas saturations, whereas the gas saturations in the overburden rocks of the well drilled outside the chimney are low throughout the section.

The fluid overpressure in the Tommeliten field is 18 MPa, which is equivalent to a fluid pressure gradient of 1.58 g/cm^3. This high fluid pressure demonstrates that the caprocks have significant sealing potential, and should have sufficiently small pore throat to prevent leakage through the pore network by Darcy flow, provided that the caprocks are water wet (Nordgård Bolås et al., 2005).

The fracturing of the reservoir rocks, the late salt movement, and the inhomogeneous gas saturation within the chimney in combination suggest that leakage through a fracture network in the caprock resulted in the gas distribution that caused the deterioration of the seismic signals. If such leakage took place, then gas would be fed to the fracture network during leakage. Then, presumably, this gas would later diffuse from the fractures into the unfractured host rock.

Repeated episodes of salt movement would replenish the fractures with gas, most likely as a slow process that did not necessarily empty the underlying reservoir as it happened. If so, then the pore pressure of the leaking gas has not necessarily been significantly above the pore pressures of the host rock. This scenario is the basis for the forthcoming modeling of the seismic chimney at Tommeliten Alpha.

A GAS CHIMNEY MODEL

We base our model on the following assumptions:

- The caprock is intersected by a fracture network.
- Gas is supplied to the fracture network at a constant rate.
- Gas diffuses from the fractures to the nearby unfractured rocks.

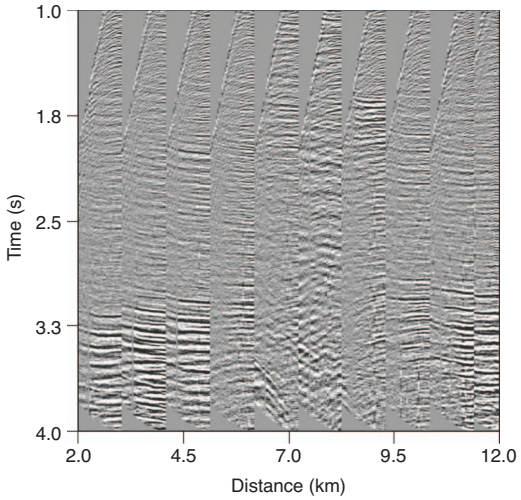

Figure 2. Moveout corrected CMPs from Statoil's research 2D seismic line across the Tommeliten Alpha gas chimney. The CMPs are evenly spaced at every kilometer starting at a distance of approximately 5000 m from the right-hand side of Figure 1.

The volume fraction of gas S in an arbitrary position x and at time t after the start of gas supply to the fractures is given by the expression (equation A-2 of Appendix A)

$$S(\mathbf{x},t) = \int d\mathbf{x}'\, s(\mathbf{x}')\frac{H_0}{8\pi DR}\left[1 - erf\left(\sqrt{\frac{R}{4Dt}}\right)\right]. \quad (1)$$

Here R denotes distance ($R^2 = (x - x')^2 + (y - y')^2 + (z - z')^2$). The function $s(\mathbf{x})$ describes a fracture network and is equal to one for a position $\mathbf{x}$ on a fracture belonging to the fracture network and zero elsewhere. H_0 is the amount of gas per time unit injected from the fracture network into the shale formations at each point of the network. Time is denoted by t, and D is the diffusion constant, which we assume to be constant.

The error function erf is given by the integral

$$\mathrm{erf}(x) = \sqrt{\frac{2}{\pi}}\int_0^x du\, \exp(-u^2). \quad (2)$$

The fracture network shown in Figure 4 was used to compute the gas saturation in the overburden of the reservoir. The network was created by computing several partial fracture networks, where each partial network was generated by first selecting a starting point for the first fracture at the top of the dome-shaped reservoir and then randomly assigning a fracture length and a fracture angle with respect to the vertical. The fracture length and fracture angle have equal probability of occurrence within an interval of 100 m and within 45° with the vertical.

The partial network was then computed recursively from the first fracture by using the endpoint of the previously generated crack as the starting point for the next, assigning randomly the fracture length and fracture angle for each new crack as described above for the first fracture. Several partial networks were then superimposed to give the network shown in Figure 4, comprising a total of 2400 individual fractures.

The presence of gas in the sediments changes the effective bulk modulus of the shale formations from K_s to K given by (Domenico, 1977)

$$\frac{1}{K(\mathbf{x},t)} = \frac{1 - S(\mathbf{x},t)}{K_s} + \frac{S(\mathbf{x},t)}{K_g}, \quad (3)$$

where K_g is the gas bulk modulus.

The density also is changed by the gas saturation and is given by

$$\rho(x,t) = [1 - S(\mathbf{x},t)]\rho_s + S(\mathbf{x},t)\rho_g, \quad (4)$$

where ρ_s is the density of the shale, whereas ρ_g is the gas density. The bulk modulus and density of the gas are dependent on the pore pressure and temperature and can be calculated from the expressions given in Mavko et al. (1998, p. 216).

The compressional and shear wave velocities now are given by

$$V_p(\mathbf{x},t) = \sqrt{\frac{K(\mathbf{x},t) + (4/3)G}{\rho(\mathbf{x},t)}},$$
$$V_s(\mathbf{x},t) = \sqrt{\frac{G}{\rho(\mathbf{x},t)}}. \quad (5)$$

The shear-modulus G is not dependent upon the fluid properties; therefore, the shear-velocity V_s depends only on the density. Figure 5 shows the compressional velocity as a function of gas saturation in a shale for different pore pressures at a constant temperature of 48 °C. The density here is equal to 1900 kg/m^3. Because of the large gas compressibility even at high pore pressures, the velocity is seen to be significantly influenced by even small amounts of gas.

The presence of fractures without any gas charge will lead to anisotropic compressional and shear wave velocity fields (Coates and Schoenberg, 1995) in the vicinity of the fractures. This will cause fluctuations in the velocity fields in addition to the fluctuations caused by the diffusion of gas from the fractures. In the following ex-

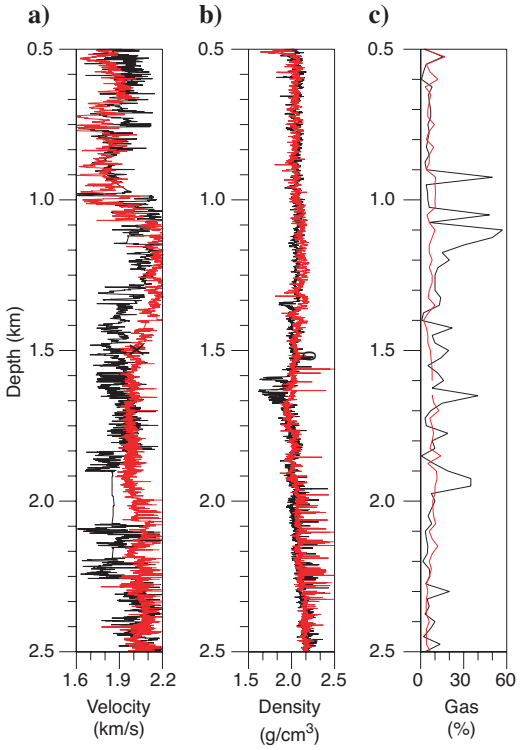

Figure 3. (a) Sonic velocity, (b) density, and (c) mud gas readings inside (black) and outside (red) the Tommeliten Alpha gas chimney.

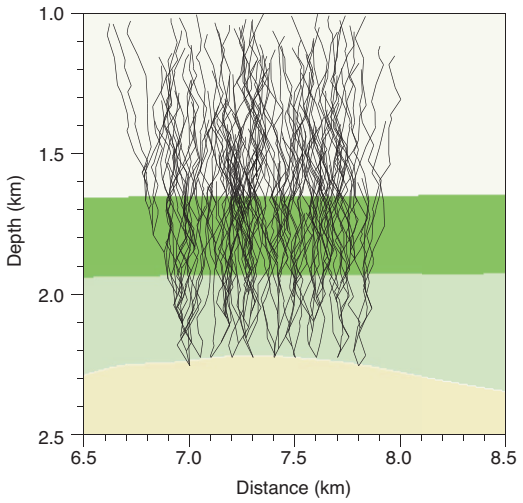

Figure 4. Fracture network overlayed on velocity field. A gas reservoir is located in the dome-shaped layer below 2300 m.

ample, this effect is neglected because the primary objective is to study the effects of gas saturation.

We used a diffusion coefficient of 10^{-12} m^2 s^{-1} as a base case value for our computations (Kroos, 1988). The gas supply rate H_0 was set to $(8\pi D)^{-1}10^{-3}$, corresponding to a gas flux of 0.01×10^9 m^3 of gas per million years for the fracture network shown in Figure 4. The pore pressure is set equal to $p = \rho_w g z$, where the water density ρ_w is equal to 1000 kg/m, the gravitational acceleration g is equal to 9.81 m/s^2, and z is the depth, whereas the temperature gradient is equal to 30°C km^{-1}.

SYNTHETIC SEISMIC DATA

An elastic finite-difference program was used to generate 230 synthetic shots using the velocity model shown in Figure 6. This velocity model was created to broadly represent the velocity field along a seismic line over the Tommeliten Alpha field. The source used in the simulation is a Ricker wavelet with maximum frequency of 50 Hz positioned at a depth of 5 m. The shot interval is 50 m, whereas the receiver spacing is equal to 25 m with a total of 120 receivers. The streamer was located at a depth of 5 m.

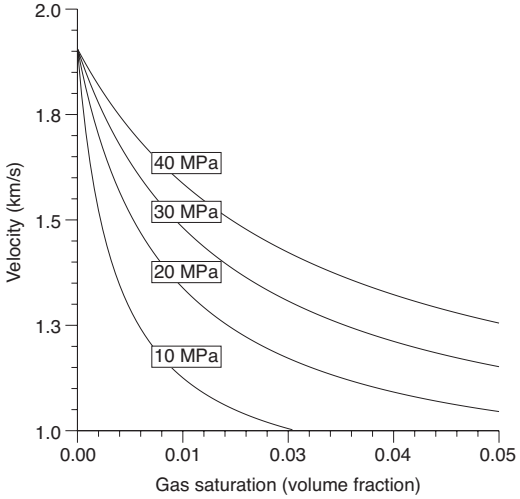

Figure 5. Seismic velocity as a function of gas saturation and pore pressure at a constant temperature of 48°C.

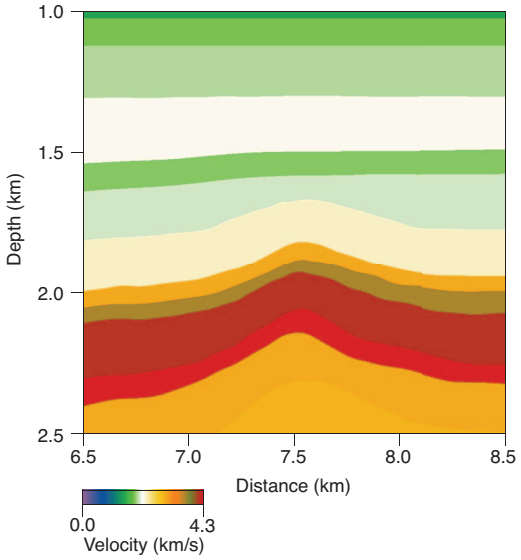

Figure 6. Background seismic velocity model not influenced by gas diffusion from the fracture network.

Figure 7 shows a prestack depth migrated section of the synthetic data. No attempt has been made to attenuate multiples present in the synthetic data. The migration was performed in the shot domain using a finite-difference explicit migration algorithm (Holberg, 1987). This algorithm is designed to take lateral velocity changes into account and is accurate for dip angles up to approximately 70°. The velocity model used for the migration was exactly the same model as that used for the modeling, and no additional smoothing of the velocity field was introduced.

The gas saturation computed from equation 1 is based on the fracture distribution shown in Figure 4, and the associated saturation and compressional velocity are displayed in Figures 8 and 9, respectively. The time from the formation of the fracture system was set to 10 million years. This velocity field was merged with the velocity field shown in Figure 6, and finite-difference modeling was used to create synthetic data with the same source and receiver parameters as described above.

Figure 10 shows the resulting seismic depth section where the velocity field used for the prestack depth migration is the background velocity model shown in Figure 6, and the migration algorithm is described above.

Significant deterioration of the seismic section is evident in Figure 10 resulting from the presence of gas diffusing from the fracture network and into the shale. The main effect of the gas present in the sediments is to reduce the compressional velocity close to each individual fracture, creating a strongly fluctuating velocity field. Because the fracture network is characterized by a typical fracture length of approximately 50 m, velocity fluctuations occur on a scale comparable to seismic wavelengths. A wave passing through such a velocity field will effectively be disrupted, thereby destroying the coherency of the wavefront.

Figures 11 and 12 show the sections of synthetic data computed with the same parameters as those shown in Figure 10, with the exception that the gas saturations and resulting compressional veloci-

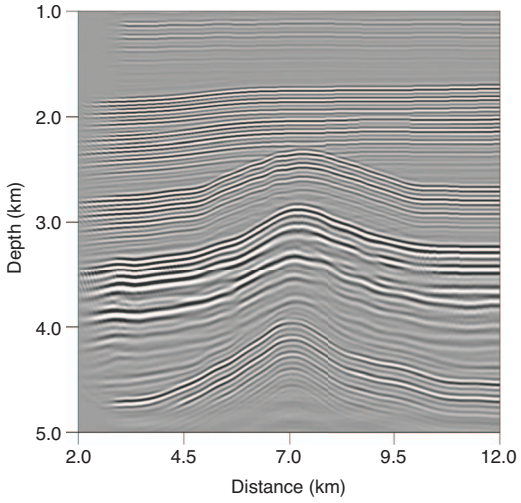

Figure 7. Seismic depth section of synthetic data computed using the background velocity field shown in Figure 6.

ties were computed 1 and 100 million years after the formation of the gas-filled fracture network. These sections suggest that the time scale of the deterioration of the seismic sections is of the order of millions of years after the fracture formation, reflecting the fact that diffusion of gas from fractures and into shale is a process with a large time scale. Initially, the gas has had little time to diffuse into the sediments and the gas saturation is low outside the fracture network (Figure 11), whereas after 10 million and 100 million years (Figures 10 and 12) sufficient time has passed to allow the gas to diffuse into the sediments and create zones of low velocities.

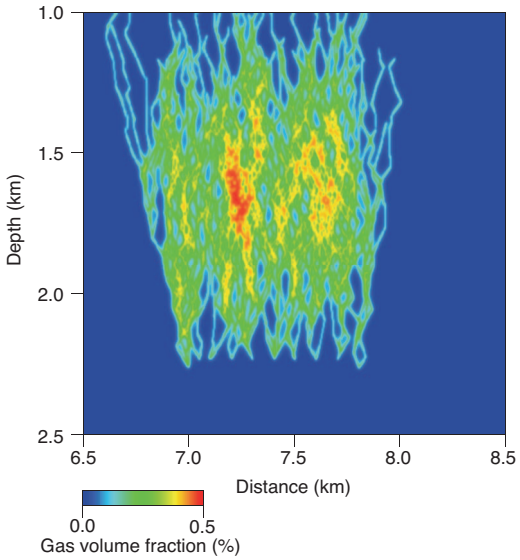

Figure 8. Volume fraction of gas for the fracture network shown in Figure 4 computed at a time equal to 10 million years after the creation of fractures.

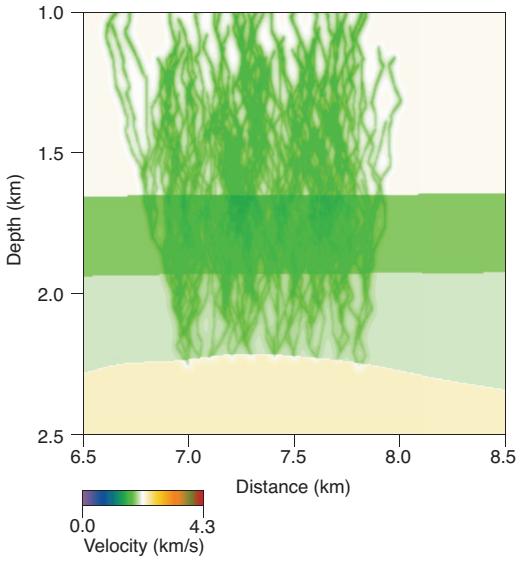

Figure 9. Seismic velocity field computed for the fracture network shown in Figure 4 at a time equal to 10 million years after the creation of fractures.

The seismic section shown in Figure 13 was computed with the same diffusion constant, fracture network, and time from creation of the fractures as the section shown in Figure 10; however, the amount of gas inserted into the network was reduced by 50%. As evident from Figure 13, this leads to a slightly less deteriorated image relative to the section shown in Figure 10 because the corresponding velocity fluctuations are smaller.

Figure 14 shows the seismic response of a fracture network with the same spatial extent as the network described above, but with an average fracture length of approximately twice that of the network shown in Figure 4. The diffusion constant, the time from the creation of fractures, and the amount of gas inserted into each point of the fracture network were the same as for the section shown in Figure 10. Because the lengths of the fractures are larger than in the case described above, the velocity fluctuations are slightly less, therefore creating a seismic section slightly less disturbed by the gas leakage than the comparable section shown in Figure 10.

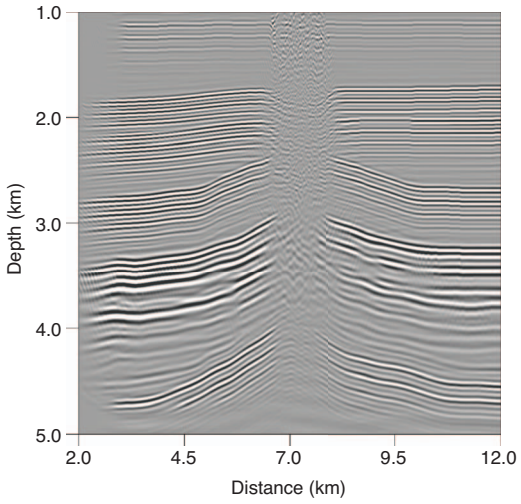

Figure 10. Synthetic seismic section computed at a time equal to 10 million years after the creation of fractures.

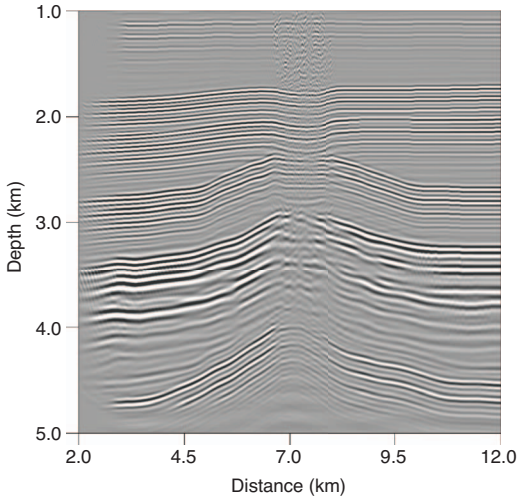

Figure 11. Synthetic seismic section computed at a time equal to 1 million years after the creation of fractures.

Figure 15 shows a seismic section migrated with the exact same velocity model as that used for modeling the synthetic data shown in Figure 10. From Figure 15 it is clear that using the exact velocity model in the migration, which includes the fluctuations in the compressional velocity because of the gas saturation, does not fully recover the true model, although the results are much improved relative to the section obtained using the background model shown in Figure 10. The main reason for not recovering the true model is the relatively short receiver array used in the generation of the synthetic data, which implies that a significant part of the scattered seismic waves from the gas chimney area is not captured. Also, the shot migration scheme used does not handle amplitudes of multiply scattered waves correctly.

COMPARISON WITH SEISMIC DATA FROM TOMMELITEN ALPHA

Figure 16 shows a raw depth migrated section of a research 2D marine seismic line acquired across the Tommeliten Alpha gas chimney and located approximately along the seismic 3D section shown in Figure 1. Migration was performed with the same algorithm described for processing the synthetic data. Also, the acquisition geometry were the same as those used for the synthetic sections. As for the synthetic data, no attempt was made to remove multiples from the real data before migration. Figure 17 shows a brute NMO stack of the same line as the one shown in Figure 16.

Although not similar in detail to the synthetic sections shown in the preceding section on synthetic data, similar features are clearly present: severely deteriorated data, time sag of reflectors, and visible diffraction tails. The synthetic sections shown in Figures 10 and 12 show the largest amount of apparent deterioration and are most similar in this respect to the real section in Figure 16.

The CMPs in Figure 2, corresponding to the stack section in Figure 17, show distorted traveltime curves of the reflections below approximately one second of two-way traveltime and total wipeout of the strong reflection from the top of the chalk formation at approxi-

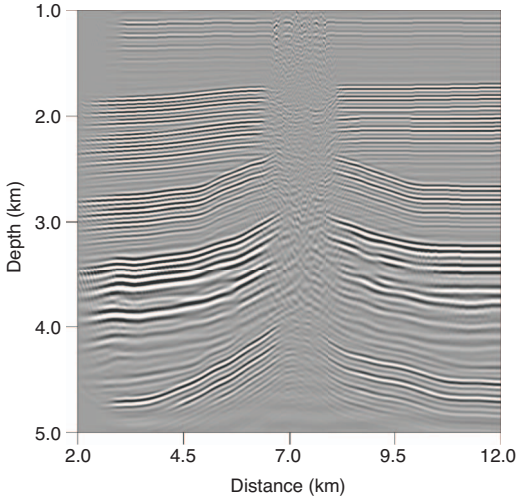

Figure 12. Synthetic seismic section computed at a time equal to 100 million years after the creation of fractures.

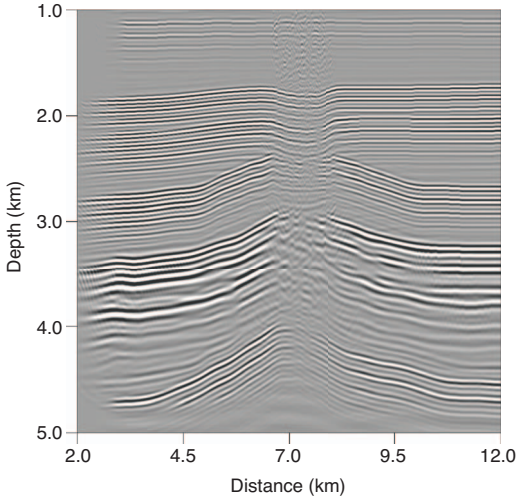

Figure 13. Synthetic seismic section computed at a time equal to 10 million years after the creation of fractures, but with reduced amount of gas injected into the fracture network.

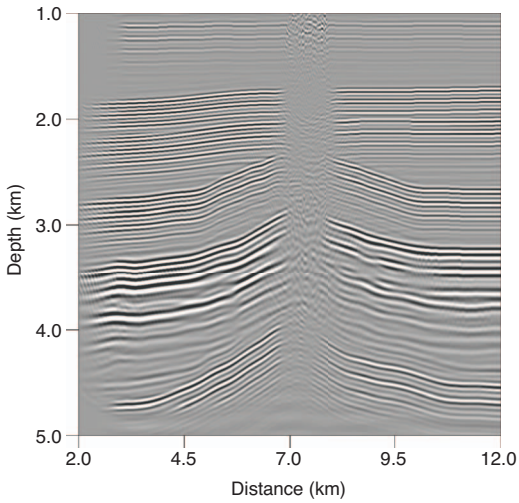

Figure 14. Synthetic seismic section computed at a time equal to 10 million years after the creation of fractures, but with an average fracture length of 100 m.

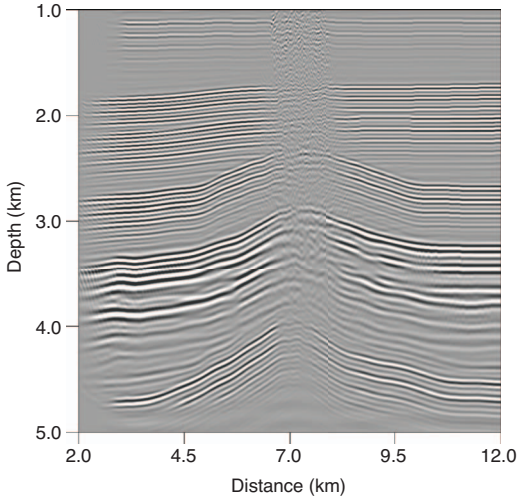

Figure 15. Synthetic seismic section computed at a time equal to 10 million years after the creation of fractures and using the exact velocity model shown in part by Figure 9.

mately 3.0 s of two-way traveltime. Also, the amplitudes of the reflections are strongly anomalous, with generally rapidly changing amplitude variation with offset. These characteristic features also are evident on the synthetic CMPs shown in Figure 18 which corresponds to the synthetic NMO-stack shown in Figure 19.

DISCUSSION

Figures 10–12 show that a simple elastic model consisting of a fluctuating compressional velocity field created by gas diffusing from a fracture network and into the sediments can qualitatively explain some of the main features of gas chimneys. The impact of the gas chimney on a passing seismic wave is, according to the proposed model, determined by the spatial distribution of the fluctuations in the velocity field and the magnitude of these fluctuations.

The fracture system itself, even without containing gas, will create fluctuations of the compressional and shear wave velocity field because of the effective anisotropy caused by the fractures. This could possibly cause scattering and distortion of the seismic wavefield in addition to the scattering caused by gas leaking into the sediments. This effect probably is of a smaller magnitude than the effect of the diffusing gas on the sediments and is neglected here. However, it is straightforward to include this effect by using the methodology described by Coates and Schoenberg (1995).

The modeling results depend on the diffusion constant (D), the gas supply rate (H^0), the fracture spacing, and the time after formation of the gas-filled fractures. In addition, the choice of constant temperature and pressure gradient, as well as a constant diffusion coefficient, influences our results. Measurements of the diffusion constants are available for different rock types, and the temperature, pressure, and time from the formation of the fractures are in many cases known. However, the gas supply rate and fracture spacing are not well known. Because the observed seismic data depend on these parameters, estimates of the parameters could, in principle, be obtainable from the seismic data itself, but more work would be needed to investigate the feasibility of this.

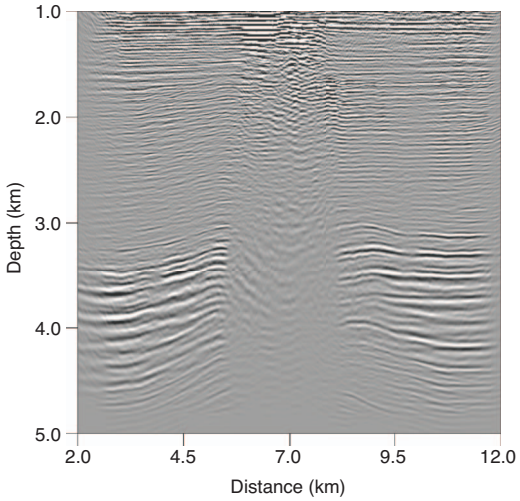

Figure 16. Raw prestack depth migration of the Statoil Research line across the Tommeliten Alpha field.

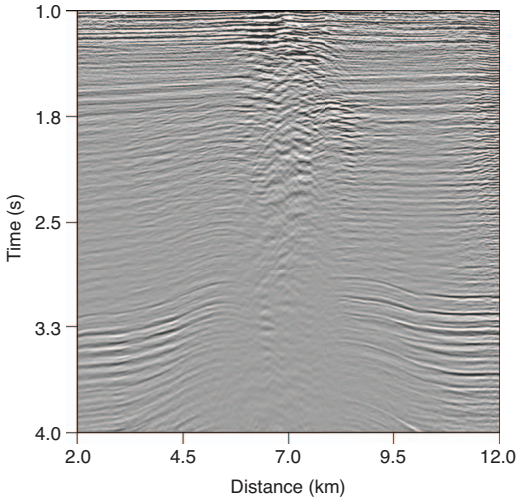

Figure 17. Raw NMO-stack of the Statoil Research line across the Tommeliten Alpha field.

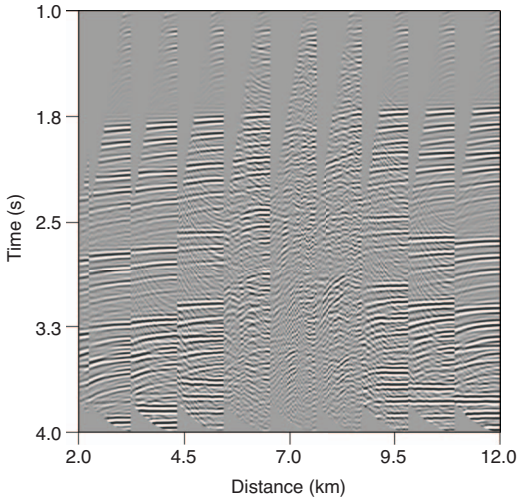

Figure 18. Moveout corrected synthetic CMPs using the velocity field shown in Figure 6.

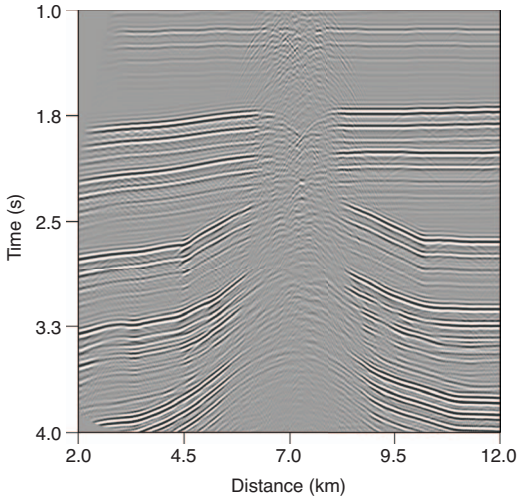

Figure 19. Raw stack of synthetic seismic data at a time equal to 10 million years after the creation of fractures and using stacking velocities obtained from the background velocity model shown in Figure 6.

The synthetic data discussed above demonstrate that the formation of a modeled seismic chimney, although with apparently different characteristics, takes place for a reasonably broad range of fracture network parameters, gas supply rates, and times.

The modeling results are most perturbed by a reduction in the gas injection rate, suggesting that a minimum gas flux is needed to provide enough gas for the velocity changes to be significant. The flux rate of our base case is approximately 0.1% of the trapped gas in the Tommeliten Alpha structure per million years. Because only a small portion of the gas that is generated in sedimentary basins is actually trapped, we feel that the flux rates of our simulations are not unrealistically low. Having said so, we acknowledge the fact that the gas leakage rate can hardly be measured or independently verified.

The modeling also demonstrates that a minimum time, in the order of a million years, is required for the gas to diffuse into the host rock of the fractures. The actual time dependence will vary with the diffusion constant.

The comparatively low diffusion constant value that was selected in our modeling suggests that the time after leakage in most cases should be sufficient to allow for the formation of clearly visible seismic chimneys.

The simplifying choices of constant temperature and pressure gradients do not significantly perturb our modeling results. This is so because these parameters are presumed to vary smoothly in the caprocks of the investigation, which would only result in smooth subsurface velocity variations. Errors in the absolute values of the pressure and temperature gradients would change the difference between the velocity of sediments and the velocity of gas, and would influence the modeling results. The inaccuracies in the velocity of gas resulting from uncertainties in subsurface pressure and temperature, however, are small compared to the velocity contrast between gas and sediments, and should thus be of minor importance. Note also that the modeled deterioration of the seismic signals occurs immediately below the top of the gas-saturated fracture network, where the errors in subsurface fluid pressure are the least.

The gas diffusion constant in sediments depends on the pore throat radii, which correlate with the permeability of the rock (Krooss et al., 1988). The matrix permeability of a caprock sequence like that above the North Sea chalk fields probably varies by several orders of magnitude. The fact that we selected a constant diffusion coefficient for our modeling implies that our modeling has underestimated the magnitude of the fluctuations, or the "patchiness" of the caprocks' gas saturation.

Several factors thus suggest that gas-filled fracture networks could result in deterioration of seismic data, including (1) the base case modeling results, (2) the comparatively small sensitivity to parameter changes, and (3) our underestimation of the patchiness of the gas saturation resulting from the selection of a constant diffusion constant. These observations, and the velocity and gas saturation differences that were observed between well 1/9-1 (outside the chimney) and well 1/9-3R (within the chimney), validate the idea that leakage through a fracture network can have caused the seismic chimneys above the chalk fields of the North Sea.

One cannot dismiss the possibility that other leakage processes can result in similar gas distributions as those resulting from our modeling. A possible mechanism proposed by Heggland (2005) and Walraven et al. (2004) involves gas migrating through faults. If gas diffuses from the fault plane and into surrounding sediments, a zone with reduced compressional velocity might be created and might possibly create an observable effect. However, the lateral extent of the resulting gas chimney should be limited to an area around the fault.

The model for the fractures and the finite-difference wave propagation is 2D, which is an accurate representation of the 3D world only if the seismic source is a line source, and in addition, the gas chimney model does not change in the direction normal to the horizontal axis. In reality, these conditions will be violated to some degree, but we believe that a full 3D modeling of a gas-filled fracture system would show similar effects as the ones we have demonstrated in 2D.

CONCLUSIONS

Transport of gas from a reservoir and into the caprock through a connected fracture network followed by diffusion can qualitatively explain the appearance of so-called gas chimneys. The gas causes fluctuations in the compressional velocity field which again cause scattering and deterioration of a passing seismic wave.

Modeling of gas transport from a chalk reservoir into an overlying fractured caprock, coupled with modeling of gas diffusion from the caprock fractures into the intact rock, has reproduced the visual appearance of the seismic chimneys that are observed over several North Sea chalk fields. The modeling results are comparatively insensitive to the modeling assumptions and parameter values.

Except for the previously mentioned leaking faults, we are unaware of any other leakage process description that results in comparable seismic signal deteriorations. The modeling results thus suggest that the geological model for leakage from the chalk fields, on which the modeling was based, is valid but unproven.

It will not be possible to find a velocity model that accurately describes the velocity field of a gas-saturated caprock if the gas leaked into the caprock through a combination of flow in fractures and diffusion from these into the host rock. Even if such a velocity field could be accurately reproduced, the limited aperture used in seismic data acquisition will make a complete reconstruction of reflectors difficult.

As a result, we believe that reprocessing of compressional data cannot result in a satisfactory imaging of gas chimneys above the North Sea gas fields. Such imaging should be possible with seabed shear-wave data, provided that the fracture presence alone did not significantly alter the seismic velocity field. This topic appears to warrant further studies.

The combination of fracture network properties, the amount of gas transported by the fractures, and the product of the diffusion constant and time can possibly explain the seemingly different appearance of gas chimneys, ranging from slightly reduced quality of seismic images to massive deterioration and strongly reduced interpretability.

APPENDIX A

DIFFUSION OF GAS IN CAPROCKS

Diffusion of gas in rocks can be described by the differential equation (Carslaw and Jaeger, 1959; Barton, 1989)

$$\partial_t S(\mathbf{x},t) = D\nabla^2 S(\mathbf{x},t) + h(\mathbf{x},t), \qquad \text{(A-1)}$$

where S is the volume fraction of gas; D is the diffusion constant, and h is the injected fractional volume of gas; $\mathbf{x} = (x,y,z)$ is the position described in a right-handed Cartesian coordinate-system, and t de-

notes the time variable. Equation A-1 can be solved by (Barton, 1989)

$$S(\mathbf{x},t) = \int dt' \int d\mathbf{x}' g(\mathbf{x},t;\mathbf{x}',t')h(\mathbf{x}',t'), \quad \text{(A-2)}$$

where the Green's function g is given by

$$g(\mathbf{x},t;\mathbf{x}',t) = \frac{1}{8(\pi D\tau)^{3/2}} \exp\left[-\frac{R^2}{4D\tau}\right]. \quad \text{(A-3)}$$

Here, $R^2 = (x - x')^2 + (y - y')^2 + (z - z')^2$ and $\tau = t - t'$. The source h is specified as

$$h(x',t') = H_0 Q(t')s(\mathbf{x}'), \quad \text{(A-4)}$$

where Q is

$$Q(t') = \begin{cases} 1 & \text{if } t > 0 \\ 0 & \text{otherwise} \end{cases}, \quad \text{(A-5)}$$

and H_0 is the volume fraction of gas injected per time unit. The function $s(\mathbf{x})$ describes a fracture network and is equal to one if $\mathbf{x}$ is located on a fracture and zero elsewhere.

Integrating equation A-3 over the time variable t' gives (Carslaw and Jaeger, 1959)

$$S(\mathbf{x},t) = \int d\mathbf{x}' s(\mathbf{x}') \frac{H_0}{8\pi DR} \operatorname{erfc}\left(\sqrt{\frac{R}{4Dr}}\right), \quad \text{(A-6)}$$

where erf$c$ is defined via the error function erf:

$$\operatorname{erfc}(x) = 1 - \operatorname{erf}(x), \quad \text{(A-7)}$$

and the error function is given by the integral

$$\operatorname{erf}(x) = \sqrt{\frac{2}{\pi}} \int_0^x du \exp(-u^2). \quad \text{(A-8)}$$

REFERENCES

Barton, G., 1989, Elements of Green's functions and propagation: Oxford Univ. Press, Inc.

Carslaw, H. S., and J. Jaeger, 1959, Conduction of heat in solids: Oxford Univ. Press, Inc.

Coates, R. T., and M. Schoenberg, 1995, Finite-difference modeling of faults and fractures: Geophysics, **60**, 1514–1527.

Dangerfield, J. A., 1992, Ekofisk field development, Making images of a gas obscured reservoir, *in* R. E. Sheriff, ed., Reservoir Geophysics: SEG, 98–109.

D'Heur, M., 1987, Albuskjell, *in* A. M. Spencer, ed., Geology of the Norwegian oil and gas fields: Graham & Trotman Ltd., 39–50.

D'Heur, M., and L. J. Pekot, 1987, Tommeliten, *in* A. M. Spencer, ed., Geology of the Norwegian oil and gas fields: Graham & Trotman Ltd., 117–128.

Domenico, S. N., 1977, Elastic properties of unconsolidated porous sand reservoirs: Geophysics, **42**, 1339–1368.

Fraser, R. H., M. D. McCormack, H. D. Johnson, J. Underhill, G. Kadolsky, R. Conell, P. Johanessen, and R. Ravnås, 2002, Upper Jurassic, *in* D. Evans, C. Graham, A. Armour, and P. Bathurst, eds., The millenium atlas, Petroleum geology of the central and northern North Sea: The Geological Society, 157–189.

Granli, J. R., B. Arntsen, A. Sollid, and E. Hilde, 1999, Imaging through gas-filled sediments using marine shear-wave data: Geophysics, **64**, 668–677.

Heggland, R., 2004, Hydrocarbon migration and accumulation above salt domes — Risking of prospects by the use of gas chimneys: Presented at the 24th Annual Gulf Coast Section, SEPM.

———, Using gas chimneys in seal integrity analysis: A discussion based on case histories, *in* P. Boult and J. Kaldi, eds., Evaluating fault and caprock seals, AAPG Hedberg Series, 237–245.

Holberg, O., 1988, Towards optimum one-way propagation, Geophysical Prospecting, **36**, 99–114.

Krooss, B. M., D. Leythaeuser, and R. G. Schaefer, 1988, Light hydrocarbon diffusion in a caprock: Chemical Geology, **71**, 65–76.

Lerche, I., 1986, Multiple scattering of seismic waves, variable gas saturation and zods: Theoretical considerations and an observational methodology: Geophysical Journal of the Royal Astronomical Society, **86**, 241–261.

Ligtenberg, J., 2003, Unraveling the petroleum system by enhancing fluid migration paths in seismic data using neural network pattern recognition techniques: Geofluids, **3**, 255–261.

Mavko, G., C. Mukerji, and J. Dvorkin, 1998, The rock physics handbook: Cambridge University Press.

Meldahl, P., R. H. R. Bril, P. de Groot, and F. Aminzadeh, 2002, Identifying seismic objects by their texture, orientation and size: A new interpretation tool: Presented at the AAPG Annual Convention and Exhibition.

Michaud, F., 1987, Eldfisk, *in* A. M. Spencer, ed., Geology of the Norwegian oil and gas fields: Graham & Trotman Ltd., 89–105.

Muns, J. W., 1985, The Valhall field: A geological overview: Marine and Petroleum Geology, **2**, 23–43.

Norbury, I., 1987, Hod, *in* A. M. Spencer, ed., Geology of the Norwegian oil and gas fields: Graham & Trotman Ltd., 107–116.

Nordgård Bolås, H. M., C. Hermanrud, and G. Teige, 2005, Seal capacity estimation from subsurface pore pressures: Basin Research, **17**, 583–599.

O'Brien, M., D. N. Whitmore, S. Brandsberg-dahl, J. T. Etgen, and G. E. Murphy, 1999, Multicomponent modelling of the Valhall field: Presented at the 61st Annual Conference and Exhibition, EAGE.

Pekot, L. J., and A. G. Gregory, 1987, Ekofisk, *in* A. M. Spencer, ed., Geology of the Norwegian oil and gas fields: Graham & Trotman Ltd., 73–87.

Walraven, D., F. Aminzadeh, and D. L. Connoly, 2004, Predicting seal risk and charge capacity using chimney processing, Three Gulf of Mexico case histories: 74th Annual International Meeting, SEG, Expanded Abstracts.

White, J. E., 1975, Computed seismic speed and attenuation in rocks with partial gas saturation: Geophysics, **40**, 224–232.